Available online at www.sciencedirect.com

ScienceDirect

Ceramics International 40 (2014) 3655–3665

CERAMICS INTERNATIONAL

www.elsevier.com/locate/ceramint

Optimization of rheological properties of photopolymerizable alumina suspensions for ceramic microstereolithography

Ankur Goswami[a,b], Ankit K[c], N. Balashanmugam[c], Arun M. Umarji[a], Giridhar Madras[b,*]

[a]*Materials Research Centre, Indian Institute of Science, Bangalore-560012, India*
[b]*Centre for Nano Science and Engineering, Indian Institute of Science, Bangalore-560012, India*
[c]*Central Manufacturing Technology Institute, Bangalore-560022, India*

Received 4 July 2013; received in revised form 12 September 2013; accepted 13 September 2013
Available online 19 September 2013

Abstract

Microstereolithography (MSL) is a rapid prototyping technique to fabricate complex three-dimensional (3D) structure in the microdomain involving different materials such as polymers and ceramics. The present effort is to fabricate microdimensional ceramics by the MSL system from a non-aqueous colloidal slurry of alumina. This slurry predominantly consists of two phases i.e. sub-micrometer solid alumina particles and non-aqueous reactive difunctional and trifunctional acrylates with inert diluent. The first part of the work involves the study of the stability and viscosity of the slurry using different concentrations of trioctyl phosphine oxide (TOPO) as a dispersant. Based on the optimization, the highest achievable solid loadings of alumina has been determined for this particular colloidal suspension. The second part of the study highlights the fabrication of several micro-dimensional alumina structures by the MSL system.

Keywords: Microstereolithography; Alumina; Rheology; Ceramic processing; Fractal analysis

1. Introduction

Microfabrication of both polymer and ceramic structures has become important since the introduction of non-silicon based MEMS technology over the last decade [1]. Different fabrication methodologies have been patented and commercialized for fabricating polymer structures in microdimensions for various applications [2]. However, the microfabrication of 3D complex ceramic structures has not been significantly explored. Though there are several methodologies and techniques (Stereolithography (SLA), Fused deposition modelling (FDM), Ink jet printing etc.) [3,4] that have evolved to create 3D complex structures, very few techniques have been successful in creating complex ceramic structures in microdomains [5,6]. Microstereolithography (MSL) is one such technique, which has been used in recent years for the microfabrication of ceramic structures [7–9].

MSL is a rapid prototyping technique which involves freeform layer by layer microfabrication of photopolymerizable liquid resin when selectively exposed to UV (preferably laser) irradiation [10,11]. Ceramic microfabrication by the MSL is carried out by blending nano to micron (mean particle size d_{50} ~ 200 nm to 2 μm) sized ceramic particles with the photopolymerizable monomer containing an appropriate amount of photoinitiator, dispersant and diluents at an optimized solids loading. This is termed ceramic resin [12]. During the operations of MSL, wherever the laser strikes the resin, it photopolymerizes and entraps the suspended ceramic particles forming a near net shape green ceramic body [13], which can be realized by successive debinding and sintering operation [14]. However, there are few major issues, which need to be addressed for achieving dense solid structures with moderately low dimensional shrinkage [13].

In order to achieve low dimensional shrinkage after debinding and sintering, ceramic particles should be loaded in the monomer suspension at an optimum amount. However, in a highly loaded ceramic suspension, viscosity increases drastically and makes it inconvenient to handle. This happens because of the inter-particle attraction due to the van der

*Corresponding author. Tel.: +91 80 2293 2321.
E-mail addresses: giridhar@chemeng.iisc.ernet.in, giridharmadras@gmail.com (G. Madras).

0272-8842/$ - see front matter © 2013 Elsevier Ltd and Techna Group S.r.l. All rights reserved.
http://dx.doi.org/10.1016/j.ceramint.2013.09.059

Waals (vdw) interaction between the neighboring particles [15,16]. The repulsive inter-particle forces create colloidally stable suspensions by reducing the vdw forces in the powder suspension to achieve the low viscosity. Therefore, the rheology of the suspension plays an important role in determining the colloidal stability of the ceramic suspension [17].

The repulsive inter-particle forces can be manipulated mainly by the introduction of electrostatic or steric forces. The former is limited mostly to the polar media where the dispersion can be stabilized by controlling the solvent pH [18]. The latter plays a dominant role in both polar and apolar media where dispersion is stabilized either by introducing extended chain diblock copolymers or short chain dispersants [15].

The rheological behavior of different volume fractions of alumina suspensions was studied in trimethylol propane triacrylate (TMPTA) and 1,6 hexane diol diacrylate at 20:80 (v/v respectively) mixture (TH2080). This was to determine the optimum volume fraction for the microfabrication of alumina structure by the MSL. After the realization of the near net shape, it is important to remove the polymer by a thermally activated process, which becomes the binder for the green ceramic body. This debinding process should be diffusion controlled to ensure a defect free structure. TMPTA is a highly viscous monomer (130 mPa s) with low polymerization shrinkage (11.5 vol%) whereas HDDA shows high shrinkage (22.7 vol%) upon polymerization with low viscosity (9 mPa s). However, after polymerization, diffusion controlled degradation upon heat treatment in inert atmosphere is observed for HDDA but not for TMPTA. We have proposed in our earlier work [19] that TH2080 is an ideal composition in terms of viscosity, shrinkage and degradation mechanism for MSL based ceramic microfabrication. Therefore, we extend our study of the rheology of alumina suspension and its microfabrication by MSL using this particular copolymer composition.

In order to ensure the maximum dispersion of these alumina suspensions in TH2080 monomer, trioctyl phosphine oxide (TOPO), was chosen as the dispersant. TOPO has an anchoring head group of phosphorous with extended tail of octyl group (as shown in Scheme 1) and has been used because of its dipolar phosphorus oxygen bond, which can easily bind with metal ion of alumina while the octyl group has an affinity to low polar media like monomer and aprotic solvent. In addition, high boiling and low viscous solvent has been used to reduce the viscosity of the suspension. Therefore, decalin has been chosen as a solvent based on the above properties [20].

The objective of this study was threefold. The first objective was to determine the TOPO concentration to ensure the stability of the alumina suspension in the above resin (TH2080). The second objective is to achieve the highest solid volume fraction at moderately low viscosity (≤ 10 Pa s) at medium shear rate (40–50 s^{-1}). In order to ensure the stability of the suspension, the concentration of TOPO was varied at different weight fractions and the best concentration was determined by sedimentation studies and fractal analyses. Thixotropic characterization was used to support the sedimentation and fractal analysis for choosing the best concentration of TOPO. Once the TOPO concentration was optimized, further studies were carried out to ensure the highest achievable volume fraction of alumina loading in this monomer solvent suspension. Further, the viscosity was determined as a function of solids loading and temperature for these suspensions. This was fitted to the Liu model [21] in order to determine the highest achievable theoretical solid volume fraction. The final objective of this study was to use the optimized solids loading and fabricate few alumina structures by the MSL system.

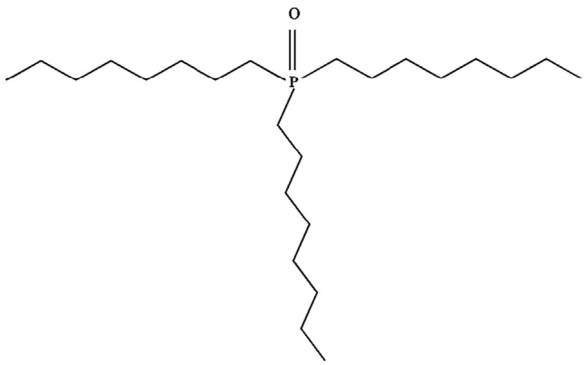

Scheme 1.

2. Experimental details

2.1. Materials

The details of the materials and their sources are listed in Table S1 (see supplementary information). The size distribution, surface area and the density of the alumina powder used in this study are $d_{50} \sim 0.5$ μm, $d_{90} \sim 2.9$ μm and 8.9 m^2 gm^{-1} (BET), 3.98 g cm^{-3}. HDDA, TMPTA monomers, TOPO and decalin were used without any further purification. BP was used after it was twice recrystallized from ethanol (EtOH). TH2080 monomer solution was prepared by mixing TMPTA and HDDA at 20:80 vol% at 25 °C.

2.2. Slurry preparation

Before the preparation of the alumina monomer slurries, physisorbed alumina suspensions were prepared at different concentration of TOPO in EtOH. The concentration of TOPO was varied in the EtOH suspension from 0 wt% to 5 wt% of alumina. Initially, the respective concentration of TOPO was predissolved in EtOH followed by the preparation of alumina suspension. To ensure better physisorption an ultrasonic probe sonicator has been used to encapsulate the alumina particles by TOPO. After 15 min of sonication, the suspensions were kept in hot air oven at 45 °C to remove all EtOH. The dried TOPO adsorbed alumina powder was de-agglomerated by passing it through a sieve of −120 mesh. Six different concentrations of TOPO adsorbed alumina (i.e. 0 wt%, 0.5 wt%, 1 wt%, 2 wt%, 3 wt% and 5 wt% TOPO in alumina suspension) were prepared and kept in a different batch. In order to carry out rheological studies to determine the best concentration of the dispersant, 25 vol% of alumina suspension with respect to

TH2080 monomer and decalin (diluent) was prepared. The monomer (M) to diluent (D) ratio was kept at 4:1, which is termed as TD41. However, the monomer to diluent ratio was also varied for viscosity measurement and the terminology is mentioned in Table S1 (see Table in supplementary information). During the slurry preparation, the monomer–diluent mixture was stirred using a magnetic stirrer. TOPO adsorbed alumina was added incrementally to this monomer–diluent mixture and stirred vigorously (For 5 h) until a homogeneous suspension was obtained. Five suspensions of different concentrations of TOPO were prepared and subjected to the rheological studies. Once the dispersant concentration was optimized by rheological experiments, different solids loading of alumina (10 vol%, 15 vol%, 20 vol%, 25 vol%, 30 vol% 35 vol% and 40 vol%) in monomer–diluent suspensions were prepared and the optimization of solids loading was further carried out by the rheological studies. For preparing higher volume fractions of alumina (30 vol%, 35 vol% and 40 vol%), slurries were subjected to ball milling for an additional 5 h to achieve a homogeneous suspension. The steps involved in the preparation of the suspension are shown in Fig. S1 (see figure in supplementary information).

2.3. Sedimentation studies and fractal analyses

The state of flocculation can be easily monitored by a simple sedimentation experiment, which provides an estimate on colloidal stability. For non-interacting ceramic particles in a fluidic suspension, the terminal velocity (ν) of the particles is governed by the following Eq. (1).

$$\nu = \frac{(\rho - \rho_0) g d^2}{18\eta} \quad (1)$$

where d is the diameter of the particle, η is the viscosity of the fluid media, ρ and ρ_0 are the densities of the solid particles and the liquid media respectively, g is the gravitational constant.

In order to carry out the sedimentation experiments, it is important to limit the concentration of the solids media to less than 1 vol%. Eq. (1) cannot be employed above this concentration due to the introduction of reverse flow in the suspension [22]. Hence, in order to carry out the sedimentation experiments, 0.5 vol% of the alumina suspension was prepared in the mixture of TH2080 and decalin (diluent) solvent [23]. These solvent mixtures were prepared at 4:1 ratio (monomer:diluent) to compare with the rheological studies where a similar solvent mixture was used. Different concentrations of TOPO treated alumina suspensions were prepared and kept in six different measuring cylinders of 10 ml volume with a lid at the same time and left undisturbed for 1.5 Ms (~17 days). All the measuring cylinders were calibrated for volume against height with the same solvent from a standard buret. Data were taken at definite time intervals (in this case 86.4 ks–24 h interval) from the mark of the measuring cylinder up to which supernatant solution is observed.

Fractal analyses have been also adopted in order to quantify the dispersion of different concentrations of TOPO treated alumina suspension using microscopic imaging of the drainage films developed on the glass microscope slides. Before beginning the experiment, glass slides were cleaned in piranha solution (H_2O_2: H_2SO_4~(1:3)) for 24 h, dried at 120 °C for 24 h followed by purging of dry nitrogen. The slides were clean and this was confirmed by complete wetting by distilled water. Different concentrations of TOPO treated alumina suspension was dropped on the clean glass slides and were allowed to wait for 60 s to develop the characteristic pattern. Before imaging, the suspensions were further diluted to 0.2 vol% by the same solvent mixture in order to obtain clear microscopic images. Nikon LV100 optical microscope has been used to capture the images in the transmitted light mode. The images were analyzed by quantifying the isoperimetric quotient and Euler number using the image processing code in MATLAB.

2.3.1. Rheological experiments

Rheological studies were carried out by TA DHR 2 (TA instruments, New Castle DE, USA) rheometer using 40 mm parallel steel plate geometry with 1 mm gap. The slurry was kept on top of Peltier base plate that maintains a constant temperature (25 °C) during the measurement. In order to carry out the best possible dispersant concentration, 25 vol% alumina suspension containing different concentrations of TOPO was tested first. Initially, the slurry in the rheometer was subjected to a pre-shear at 10 s^{-1} for 2 min followed by a zero shear rate for 3 min. Once these two measurements were carried out, the samples were tested under oscillatory time sweep at 0.5% strain with an angular frequency of 10 rad s^{-1} for 4 min in order to determine the stability of the sample. This measurement provides the storage (G') and loss modulus (G'') of the sample that indicates the viscoelastic behavior of the sample. Subsequently, the viscosities of all the slurries were measured in an upward and downward sweep (η_{uw} and η_{dw}) with a shear rate increasing from 0.1 to 300 s^{-1}. The complete cycle of upward and downward sweeps was completed in 120 min. During the flow sweep, the steady state sensing was maintained for 3 min to collect each data.

The thixotropic behavior of the samples was examined by the viscosity measurement in upward and downward sweep. The thixotropic behavior is quantified in terms of the viscosity difference between the downward and the upward sweep i.e ($\eta_{dw} - \eta_{uw}$). The rheological studies of different volume fraction of alumina in monomer–diluent suspension were carried by varying the shear rate from 1 to 100 s^{-1} at 25 °C. In addition, the temperature dependent viscosity measurements were also performed (25–75 °C) at a constant shear rate of 45 s^{-1} for different volume fractions of the ceramic suspensions. The rheological behavior of the suspension was analyzed by Cross model and the non-linear behavior and the flow index were determined using this model. The Liu model was used to determine the highest achievable ceramic volume fraction in the suspension [24].

2.4. Microfabrication of alumina structures by microstereolithography (MSL)

The microstructure of the alumina ceramics was fabricated by the in house built scanning based MSL system. This system

consists of an argon ion laser (wavelength predominantly ~364 nm), an AOM, computer controlled XY–Z stage, optical mirrors, 0.5 mm variable aperture, UV transparent lens with a focal length of 50.2 mm. The setup is placed on the top of a vibration isolation table. The detailed description of the setup can be found in our earlier work [11]. Fig. S2 (see supplementary information) shows the schematic of this setup. Few 2D and 3D ceramic micro-components have been fabricated by this in house built MSL setup with an optimized dispersant concentration of TOPO in the presence of 0.1 wt% (of alumina weight) photoinitiator (BP). The fabricated structures were debinded and sintered after forming the net shape. Debinding and sintering protocols are the following: the green net shape ceramic bodies were heated to 120 °C at 0.3 °C min^{-1} for 30 min followed by heating to 500 °C at 0.2 °C min^{-1} and kept constant for 30 min to remove the organic content. Debinding process was carried out under N_2 atmosphere in order to avoid the exothermic decomposition of the polymer and to maintain a diffusion controlled reaction [19]. Then, the temperature was increased to 1550 °C at 15 °C min^{-1} followed by 5 h soaking period in order to obtain dense sintered alumina microceramics.

3. Results and discussion

3.1. Optimization of dispersant concentration

The optimization of dispersant concentration was carried out by three different measurement namely sedimentation, fractal analyses and rheological studies. Initially, a sedimentation experiment was performed to quantify the settling of alumina particles for different concentrations of TOPO treated suspensions. Fig. 1 shows the sedimentation plot of alumina suspension in 4:1 of TH2080 and decalin (solvent) mixture. Fig. S3 (a) and (b) (see supplementary information) show the photographs of the sedimentation of the alumina suspension for different concentrations of TOPO at $t=0$ and $t=1.3$ Ms. It is observed from Fig. S3(b) that the suspension containing 0 wt% TOPO settles faster than the higher concentrations of TOPO treated suspensions. In case of 2 and 3 wt% concentrations, the settling was observed to be much slower. However, in all the cases, a clear supernatant is observed leaving a faint boundary on the settling layer. The viscosity of the solvent mixture used in this study is 24 mPa.s at 25 °C and the terminal velocity calculated from the sedimentation data corresponds to the Stokes diameter of 120 nm and 75 nm for 0 wt% and 3 wt% TOPO treated alumina suspension, respectively. However, when the concentration was increased to 5 wt%, the corresponding Stokes diameter was found to be 100 nm. Therefore, the primary observation suggests that the effective Stokes diameter decreases with increasing TOPO concentration, due to the steric repulsion between the neighboring alumina particles. Nevertheless, after a certain concentration, the agglomeration increases because of the depletion flocculation mechanism [25]. However, suspensions are quite stable after 1500 ks (~18 days) for 2 and 3 wt% TOPO treated suspensions. In order to quantify this dispersion behavior, the following fractal analyses were carried out.

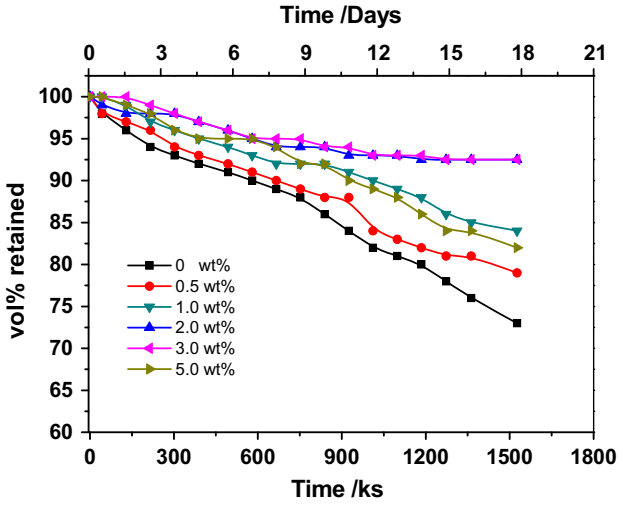

Fig. 1. Photograph of sedimentation of alumina in TD41 solvent. Fig. 1: Variation of sedimentation volume with time of alumina in TD41 solvent.

The patterns formed from the droplet of the six different suspensions of alumina containing TOPO were characterized by optical microscopy and are shown in Fig. 2(a). It is observed that the alumina suspension without TOPO has an agglomerated feature, which suggests that there was flocculation of alumina particles due to the interplay of vdw forces between the interparticles. With the addition of TOPO in the suspension, dispersion is observed to be predominant. The following image analysis technique proposed by Evans et al. was adopted for the quantification of the dispersion behavior [22].

All the images were converted to bilevel images and are shown in Fig. 2(b). It is evident from the figure that large agglomerations are formed for the poorly dispersed suspension and hence large connected black and white regions can be observed in the figure. Evans proposed that the sizes of these regions are much smaller but much larger in total numbers for the well dispersed suspension. This can be better understood from the topological concept of the Euler number [25]. For a given bilevel image, Euler number is defined as the difference between the total number of regions (summation of black and white region) and the total number of holes (total number of either white or black).

Another way of quantifying the dispersion uniformity of the images is by calculating Dido's isoperimetric quotient (Q). This quotient is defined as the ratio of the area A enclosed by curves of length L to the area of the circle of same length or perimeter (L) i.e $Q=4\pi A/L^2$ [26]. In case of a circle $Q=1$, otherwise $Q<1$. Mathematically, the regions containing more holes shows longer perimeter than its area and thus shows lower Q. Therefore, the higher uniformity of an image can be quantified by the lower Q values. Thus, the dispersion can be quantified by higher Euler number and with lower Q values for a given bilevel image.

Fig. 3 shows the plot of Euler number and the isoperimetric quotient with respect to the different concentrations of TOPO treated alumina suspensions calculated from the optical

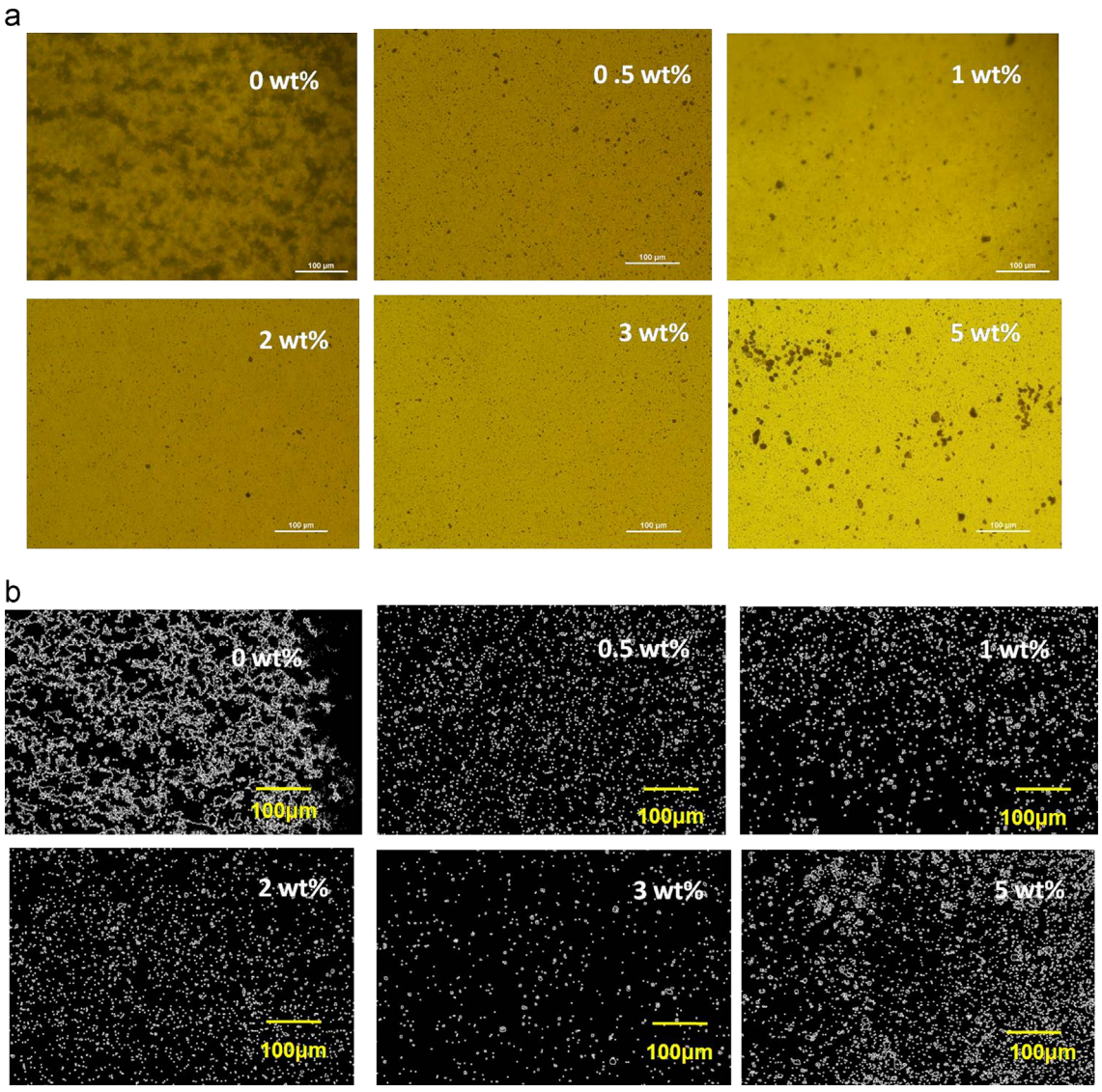

Fig. 2. (a): Optical micrograph of the drainage film of alumina in TD41 solvent (b) Bilevel image of all micrograph of the drainage film.

micrograph shown in Fig. 2(b). It is evident that 3 wt% concentration of TOPO shows lower Q values with higher Euler number. Therefore, this particular concentration shows the highest dispersion behavior. The rheological properties were studied for further confirmation.

Fig. 4(a) shows the rheological studies of different concentration of TOPO containing alumina in 25 vol% suspension in TH2080 (monomer) and decalin (solvent) (monomer:solvent ~4:1). With increasing TOPO concentration in the suspension, the viscosity decreases steadily at 3 wt% concentration of TOPO at 45 s^{-1} shear rate. Further, the increase of TOPO concentration does not lead to the significant change in the viscosity.

Fig. 4(b) shows another important characterization of dispersant concentration by thixotropic properties of the suspension, which indicates the kinetics of network formation over the experimental time. Faster restoration signifies the suspension is more stable. The restoration of the structure can be better understood by plotting the difference in viscosity during downward and upward shear rate sweep [27]. Zero difference indicates that the structure is restored

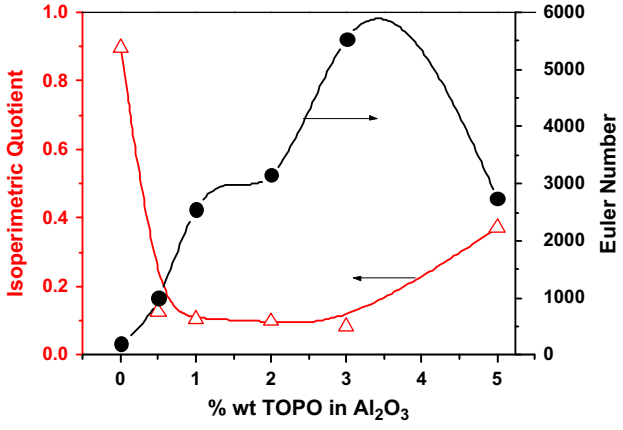

Fig. 3. Plot of isoperimetric quotient and Euler number for different concentrations of TOPO in alumina suspension.

completely within the applied shear rate whereas negative values suggest there is delay in the restoration of the network structure to the original state. It is observed from Fig. 4(b) that all the slurries

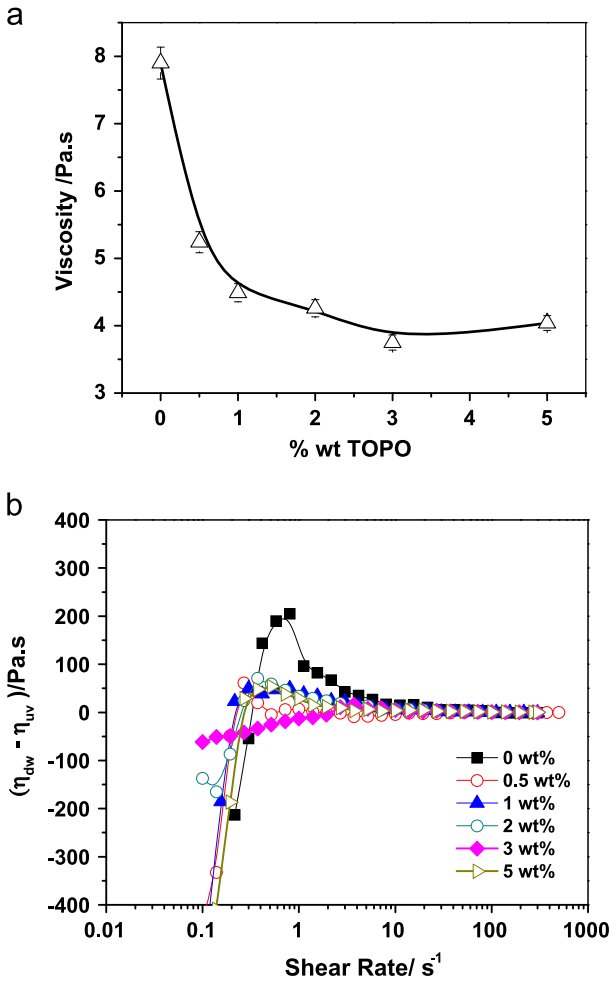

Fig. 4. (a): Viscosities of 25 vol% alumina suspension in TD41 solvent at different TOPO concentrations at shear rate of 45 s^{-1}. (b) Thixotropic behavior of the same suspensions by measuring the difference of viscosity in upward and downward shear rate sweep with the function of shear rate.

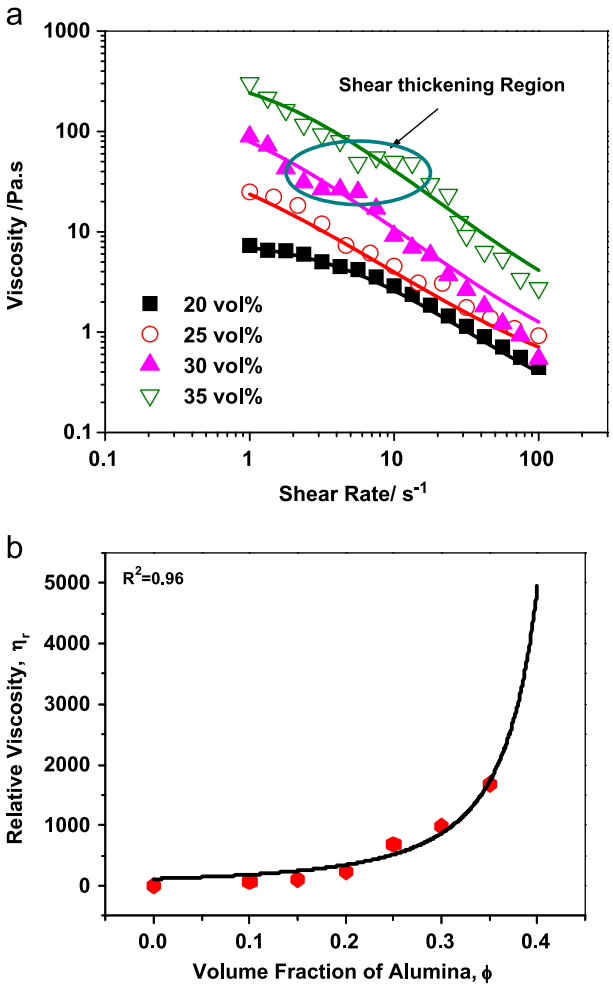

Fig. 5. (a): Viscosities of alumina suspension at different solids loading (20 vol%, 25 vol%, 30 vol% and 35 vol%) in TD41 with the function of shear rate. (b) Relative viscosities with the function of alumina volume fraction. Data are fitted to the Liu Model.

were almost restored to their original structures within 10 s^{-1}. However, at low shear rates, the restoration is delayed. 3 wt% TOPO shows the maximum recovery of the network structure and thus is an optimized dispersant for this ceramic resin.

It is observed that the suspension does not show the desirable rheological property either below or above 3 wt% concentration of TOPO. The suspension is not stable below this concentration and the dispersant remains non-adsorbed to the surface above this concentration. If the non-adsorbed dispersant concentration crosses the critical limit, the flocculation mechanism starts dominating due to osmotic effects, which is known as depletion flocculation (especially in highly concentrated suspension). Consequently, high degree of agglomeration and high viscosity is observed after the optimized concentration of the dispersant [28].

3.2. Rheological study to optimize solids loadings of alumina

The optimization of solids loading of alumina suspension in the same resin has been performed by rheological studies. Fig. 5(a) shows the shear viscosity curve with the function of shear rate for different volume fractions of alumina in the same solvent of 3 wt% TOPO. The volume fraction of alumina was varied from 20 vol% to35 vol% at an interval of 5 vol%. At this monomer to solvent ratio (4:1), the solids loading of more than 35 vol% cannot be achieved since the viscosity of the slurry becomes very high because of the moderately high continuous phase viscosity (η_c) of the slurry medium. From Fig. 5(a), it is observed that all the suspensions show shear thinning behavior. However, a slight shear thickening phenomena is observed for the intermediate shear rate regime in case of 35 vol% loading. This observation is common in monodisperse particle suspensions where, after a critical shear rate, the formation of jamming clusters occurs by hydrodynamic lubrication forces. This inhibits the motion of the particles and thus increases the viscosity [29]. Foss et al. have studied this phenomenon by Stokesian dynamics simulation using the concept of Péclet number (*Pe*) [30], which is defined as the ratio of hydrodynamic shear to the thermal forces. It is expressed as $Pe = \dot{\gamma}a^2/D$, where $\dot{\gamma}$ is the value of shear rate and $D = kT/6\tau\eta a$ is the Stokes-Einstein diffusivity of an isolated spherical particle having a radius of a and thermal

energy kT in fluid whose viscosity is $\boldsymbol{\eta}$ (in this case $\eta = \eta_c$). The occurrence of unusual behavior of shear thickening is found to be over the range of volume fraction (φ) of $0.316 \leq \phi \leq 0.49$. However, the regime of shear thickening depends on the value of *Pe*. It has been argued that for low $Pe < 10$, Brownian motion dominates the behavior thereby shear thinning is observed and the suspension is well dispersed. For higher Péclet number ($Pe > 10$), shearing force dominates over Brownian motion, which pushes the particles into close proximity where short-range hydrodynamic forces prevail. Therefore, higher forces are required to overcome this hydrodynamic force and thereby the suspension exhibits shear thickening behavior.

In case of the suspension containing 35 vol% solids loading, the estimated *Pe* number is found to be of the order of 8–9 (< 10) in the regime of 1–5 (s^{-1}) shear rate indicating the suspension has an initial shear thinning behavior. At a higher shear rate, *Pe* increases (> 10) and thus exhibits shear thickening behavior. However, at a shear rate higher than 20 s^{-1}, the suspension again shows a shear thinning phenomena because of the reduction of the continuous phase viscosity (η_c). In case of 30 vol%, shear thickening is not prominent, but a small Newtonian window is observed in the regime of 2–5 s^{-1} shear rate. This volume fraction is just lower than the limiting volume fraction ($0.316 \leq \phi \leq 0.49$) for this unusual phenomena to occur [30]. Nevertheless, all the volume fractions studied here show an overall shear thinning behavior and thus can be fitted to the Cross model (given by Eq. (2)), which is often employed to determine the shear thinning viscosity.

$$\eta = \eta_\infty + \frac{\eta_0 - \eta_\infty}{1 + (C\gamma)^m} \tag{2}$$

In Eq. (2), η_∞ and η_0 represent the asymptotic viscosities at very high and low shear rate, respectively. m is the rate constant and C is the consistency index. Essentially, $m = 0$ signifies the suspension is Newtonian, while at higher values of m (> 0.8), indicate the suspension is shear thinning.

Table 1 shows the values of different rheological parameters for different volume fractions based on the rheological analyses using the Cross model. It is observed that the asymptotic viscosity at low shear rate (η_0) increases with increasing volume fraction of the alumina particles in the suspension. This is due to the higher hydrodynamic interaction due to the increase in number of particles with increasing volume fraction of the solids loading. However, the asymptotic viscosity at high shear rate does not show any significant trend since catastrophic failure of the internal structure occurs at higher shear rate (> 50 s^{-1}). In all the cases, the exponent (m) lies in between 0.85 and 1.13. This shows that all the suspensions show shear thinning behavior and show a finite C value suggesting that all suspensions exhibits pseudo plasticity and require a critical shear rate to start the flow.

It is observed that the suspension becomes very viscous after a certain volume fraction. Hence, it is important to predict the highest theoretical volume fraction up to which the ceramic can be loaded in the suspension. Therefore, the Liu's model has been adopted [24]

Table 1
Calculated flow index from Cross model.

Vol% (Solvent)	η_0/Pa.s	η_∞/Pa.s	C	m	R^2
20 (TD41)	8.22	0.114	0.19	1.08	0.99
25 (TD41)	72.49	0.278	2.17	0.95	0.99
30 (TD41)	189.41	0.362	1.37	1.09	0.99
35 (TD41)	402.77	0.876	0.71	1.13	0.96
40 (TD11)	327.08	0.91	1.52	1.17	0.99

$$\eta_r = [a(\phi_m - \phi)]^{-n} \tag{3}$$

In Eq. (3) η_r is the relative viscosity of the suspension, which is calculated by dividing the viscosity of the suspension at particular solids loading (ϕ) by the viscosity of the suspension at zero solids loading at a given shear rate. ϕ_m is the maximum theoretical solids loading at which the viscosity of the suspension becomes infinite. a is the empirical constant and n is the flow dependent parameter, which is suspension specific. In most cases, reliable fitting was obtained at $n = 2$.

Fig. 5(b) shows the $\eta_r - \phi$ plot of alumina suspension at different solids loading fitted to the Liu's model at 45 s^{-1} shear rate. It is observed that $\phi_m = 0.47$ is the maximum theoretical volume fraction in this resin (i.e. TD41) at 45 s^{-1} at which the viscosity will be infinitely high. Therefore, the optimization of monomer to solvent ratio is important in order to achieve higher solids loading with lower viscosity.

3.3. Optimization of monomer to solvent ratio

It is observed (Fig. 5(a)) that at high solid volume fraction (~35 vol%), the suspension shows shear thickening behavior for an optimized solids loading with the particular monomer to solvent ratio (~4:1) in the intermediate shear rate. Hence, it is imperative to optimize the monomer to solvent ratio at this particular solids loading to obtain a uniform shear thinning behavior. Therefore, four rheological studies have been performed at different monomer to solvent ratio at 35 vol% solids loading. Fig. 6(a) shows the shear viscosity plot of the alumina suspension (35 vol%) for different monomer to solvent ratio. It is observed that when the ratio of monomer to solvent becomes 1:1, shear thickening diminishes and uniform shear thinning is observed. This happens because of the reduction of continuous phase viscosity (η_c) of the suspension due to the addition of more diluent (decalin). With this motivation, the solids loading was increased up to 40 vol% in which monomer to solvent volume ratio was kept 1:1 (i.e TD11). Rheology was performed at this loading (40 vol%) and it is found that the viscosity of this solids loading shows completely shear thinning behavior in the intermediate shear rate (Fig. 6(b)). This indicates the optimal volume fraction of alumina is 40 vol% for this monomer to solvent ratio (1:1) for MSL based ceramic fabrication.

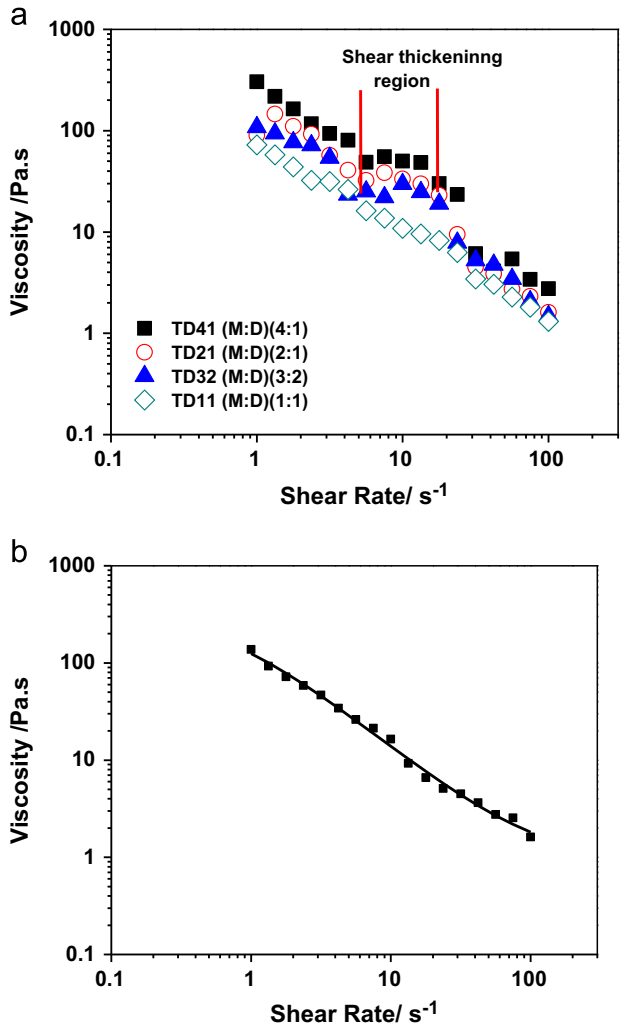

Fig. 6. (a): Viscosities of alumina suspension of fixed solids loading (35 vol%) at different monomer to diluent ratio.(b) Viscosity of alumina suspension of 40 vol% solids loading at TD11 solvent.

3.4. Effect of thermal dilution

Thermal dilution is an another method to reduce the viscosity of the suspension [20]. The viscosity of the liquid medium (both monomer and diluent) decrease as the temperature increases. This results in the decrease of continuous phase viscosity (η_c), which reduces the suspension viscosity. On the other hand, with an increase of temperature, liquids show larger thermal expansion than solids that eventually reduces the actual solids loading in the suspension. Chu et al. proposed the temperature adjusted solids volume fraction ($\varphi_{(temp)}$) by the following expression [31]

$$\phi_{(temp)} = \frac{V_s}{V_s + V_L + \Delta V_L} \tag{4}$$

The volumetric coefficient of thermal expansion of acrylate monomer is found to be of the order of $6 \times 10^{-4}\ ^{\circ}C^{-1}$ and for alumina, it is $8.1 \times 10^{-6}\ ^{\circ}C^{-1}$ [20]. Hence, the liquid media has a larger effect in the reduction of volume fraction of the ceramic particles. Therefore, $\varphi = 0.35$ volume fraction of alumina suspension at 25 °C becomes 0.34 at 75 °C and shows a significant reduction in viscosity. This happens because the viscosity is more sensitive to the volume fraction at high solids loading. Fig. 7(a) shows the reduction of viscosity at different solids loading of alumina at a heating rate of 3 °C min^{-1} at 45 s^{-1} constant shear rate. The viscosity of the suspension shows an Arrhenius dependence with temperature and can be expressed by the following Eq. (4).

$$\eta(T) = A.\exp\left(\frac{E_a}{RT}\right) \tag{5}$$

Table 2 shows the apparent activation energies (E_a) due to the reduction of viscosities with temperature at increasing volume fraction of the alumina suspensions. The activation energies significantly increase with the volume fraction in the suspension due to the reduction of solid volume with increasing temperature. The actual volume fraction at different temperatures (Eq. (3)) and corresponding relative viscosities from the Liu's model (Eq. (2)) have been calculated and listed in Table 2. It is observed that the reduction of the relative viscosity with increasing temperature is more pronounced in case of higher volume fraction suspension because of the larger increment of effective space ($\phi_m - \phi$) in the suspension. Therefore, larger E_a is observed for the suspension with high volume fraction of solids.

It is important to note the volume fraction in Fig. 7(a) has been taken as nominal volume fraction of the suspension. However, the plot of relative viscosity with the function of corrected volume fraction is shown in Fig. 7(b). It is observed that both the relative viscosity and the temperature corrected volume fraction collapse on to a single plot and can be represented by the Liu's model.

Thus, it is clear that that the high volume fraction of solid loadings can be achieved by reducing the continuous phase viscosity of the suspension. The reduction in the viscosity can be accomplished either by increasing the diluent amount in the monomer–diluent mixture or by increasing the temperature of the suspension. Since the monomer only takes part in the photopolymerization process, it is always better to keep a higher monomer concentration than the solvent to ensure better binding of the ceramic particles. Therefore, the second strategy would be more preferable to ensure better green density. To employ the second strategy, 35 vol% suspension (monomer: diluents (4:1)) can be heated in situ up to 50 °C while operating the microfabrication process by MSL. However, this will require a modification in the existing setup to include an in situ heater attachment on the slurry container. Therefore, in this study, we have employed the first strategy i.e. using 40 vol % alumina in TD11 to microfabricate the alumina structures.

3.5. Microfabrication of alumina ceramic by MSL

40 vol% of alumina in TD11 has been chosen to fabricate few simple and complex structures. BP has been used as a photoinitiator in the suspension at 0.1 wt% of the alumina loading in order to photopolymerize the suspension under laser. The exposure energy (ln E_{max}) was maintained at 10.3 J/m^2. BP was chosen since it shows lower curing width because of its low

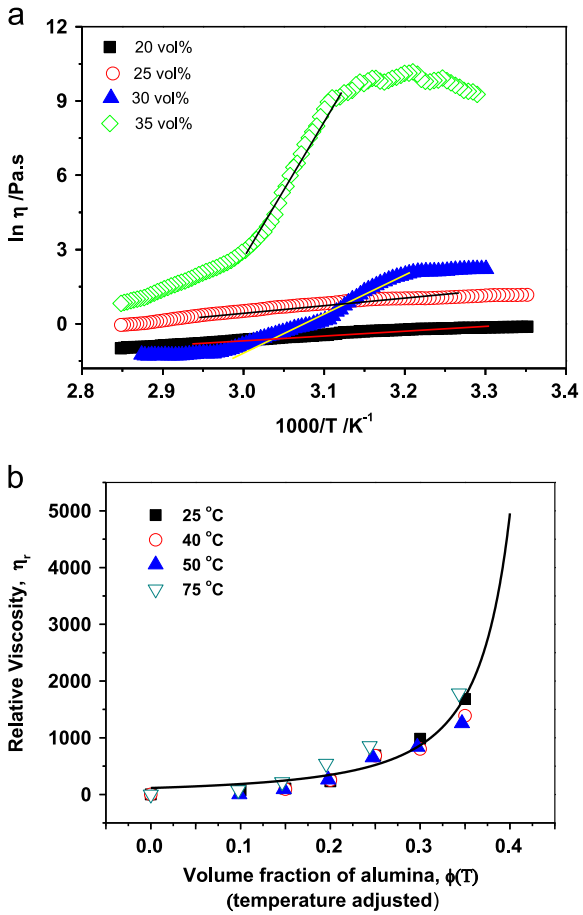

Fig. 7. (a): Temperature dependent viscosities at different solids loading (20 vol%, 25 vol%, 30 vol% and 35 vol%). (b) Relative viscosity plot with the function of alumina volume fraction at different temperatures. All the data are fitted to single the Liu model.

Table 2
Temperature adjusted solids loading of suspension (φ) at different temperature and corresponding relative viscosities (η_r).

25 °C		40 °C		50 °C		75 °C		E_a/kJ mol^{-1}
φ	η_r	φ	η_r	φ	η_r	φ	η_r	
0.2	347	0.199	344.7	0.198	342.7	0.195	334.8	15.7
0.25	521.2	0.248	512	0.247	507.4	0.243	489.9	21
0.3	868	0.298	848	0.297	838.8	0.293	801.8	120.8
0.35	1726	0.348	1670.7	0.346	1618.1	0.343	1543.7	447.5

efficiency [11]. Fig. 8(a and b), Fig. S4 (a) and (b) (see these figures in supplementary information) show the 2D net shape of the alumina green bodies. The structures are square mesh, impeller (with a central hole), crosshatch mesh, and hollow gear, respectively. The inset of Fig. 8(a) shows the porous morphology of the green ceramic object. The inset of Fig. 8(b) depicts the confocal microscope image of impeller, which shows the profile of the 2D impeller structure. Fig. 9(a)–(c) and Fig. S4 (c) (see supplementary information) show the sintered body of gear (with no hole), gear (with central hole), solid impeller and square mesh structures fabricated by the in house built MSL at 40 vol% solids

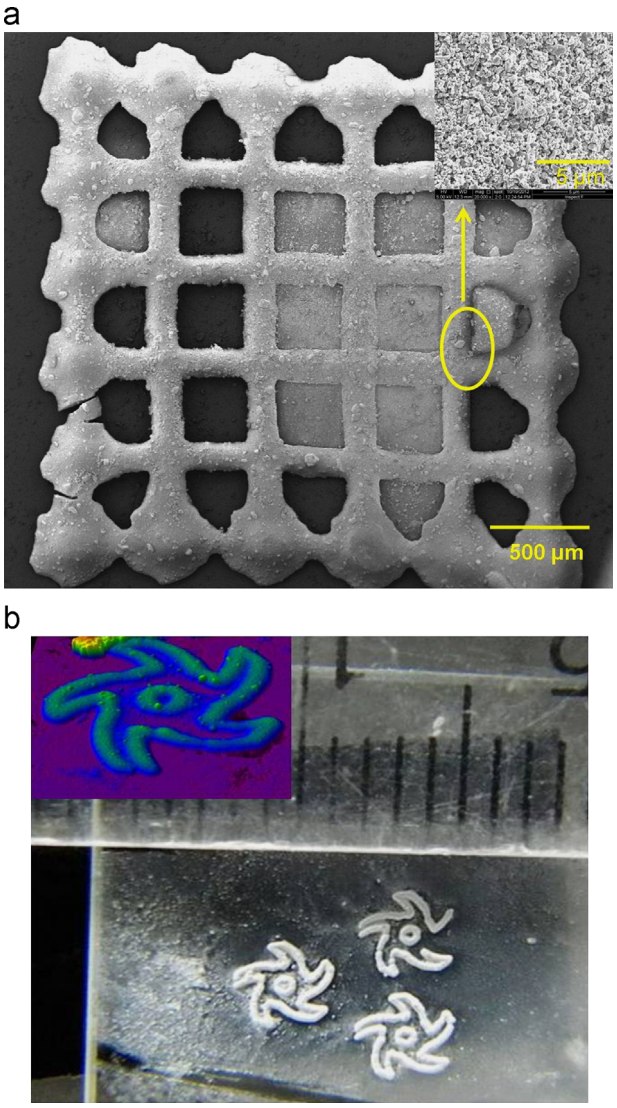

Fig. 8. Micrographs of 2D (a) square mesh and (b) impeller with a central hole. All are green bodies. Inset of Fig. 8(a) shows the porous morphology of green ceramic body. Inset of Fig. 8(b) shows the confocal image of impeller.

loading. The insets (right top corner) of Fig. 9(a)–(c) and Fig. S4 (c) (see supplementary information) show the sintered grain morphology of the gear and mesh. The insets (left bottom corner) of Fig. 9(a) and (c) show the confocal micrograph of the gear (with six teeth) and impeller (with five teeth) structures which show the 3D profile of the sintered body. The 2D structures are cured once while the 3D structures are cured thrice by laser scanning which are formed at a height of 500 µm from the base. In all the cases, the shrinkage of the structures is nearly 25–28% from its initial dimensions.

4. Conclusions

In this article, the focus was to study the colloidal behavior of alumina monomer gel for fabricating alumina microceramics by microstereolithography. The optimization of colloidal stability was demonstrated by sedimentation, fractal and rheological studies. The analysis of sedimentation and fractal

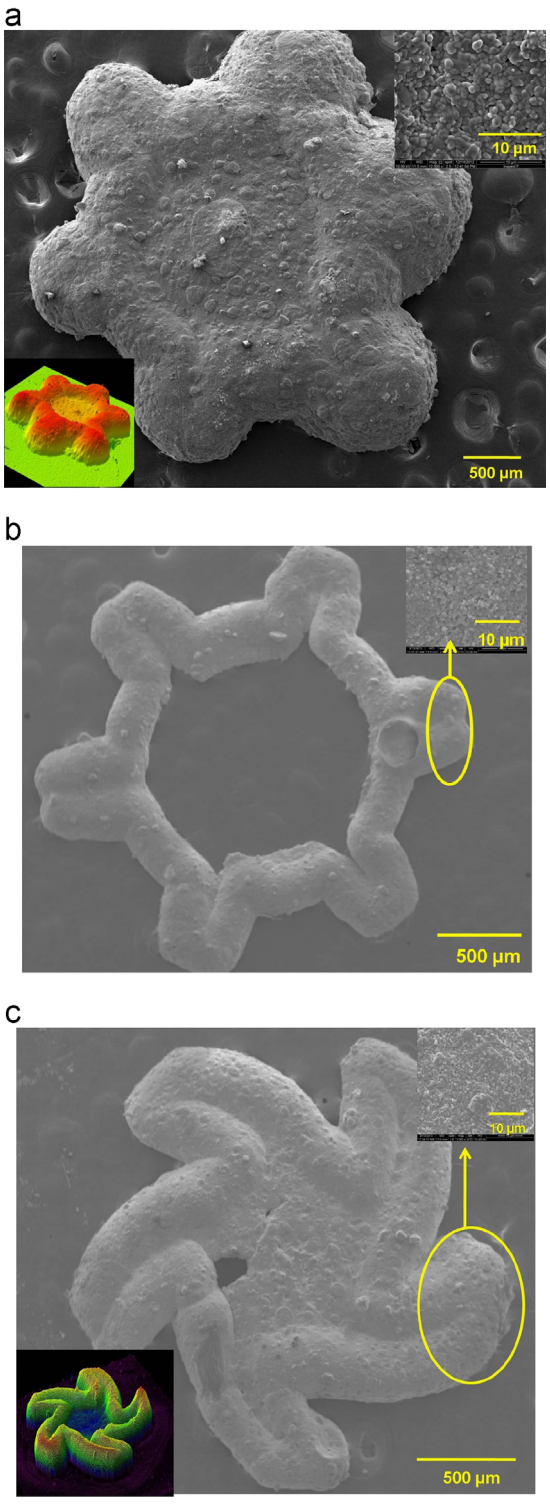

Fig. 9. Images of (a) microgear (no hole), (b) hollow gear with six teeth and (c) solid impeller fabricated by MSL. All are sintered at 1550 °C for 5 h. Inset (Right top corner) of Fig. 9 (a), (b) and (c) show the sintered morphology of all the structures. Inset of Fig. 9 (a) and (c) (left bottom) show confocal images of the gear and impeller.

studies helped in choosing the required concentration of dispersant. The rheological results were in agreement with these two experimental studies. Further, rheological studies were carried out to determine the maximum achievable volume fraction using this monomer and solvent ratio. The increment of volume fraction of alumina particles without compromising the viscosity has been demonstrated by choosing the optimum monomer to diluent ratio. The fabrication of several alumina micro-ceramics was accomplished with the optimized parameters obtained by these studies. Thermal dilution was also proposed to reduce the viscosity of the suspension at high solids loading. Further studies will examine the fabrication by modifying the MSL setup by attaching a heater for the container containing colloidal ceramics. This will help in reducing the viscosity during the process of fabrication at even higher solids loading and also reduce the post sintering shrinkage.

Acknowledgements

The authors would like to thank Centre of Excellence in Nanoelectronics (CEN) program, Indian Institute of Science (IISc) for financial support. The authors also express their gratitude to Dr. Surya Sarathi Bose from Materials Engineering Department IISc for useful discussions on rheology. Ms. Bharathi from MRC, Mr. Jagadish from CMTI and Mr. Shafique from NIT, Surathkal are gratefully acknowledged for their help in doing sample preparation, confocal microscopy and CAD design.

Appendix A. Supporting information

Supplementary data associated with this article can be found in the online version at http://dx.doi.org/10.1016/j.ceramint.2013.09.059.

References

[1] P. Dario, M.C. Carroua, N. Croce, M.C. Montesi, M. Cocco, Non-traditional technologies for microfabrication, Journal of Micromechanics and Microengineering 5 (1995) 64–71.
[2] D.J. Hansford, J. Guan, (The ohio state university), US2004/0115279A1, 17 June 2004.
[3] A. Ghosh, in: Rapid Prototyping: A Brief Introduction, East-West Press Pvt. Ltd., New Delhi, India, 1997.
[4] J.G. Calvert, R. Crockett, Chemical solid free-form fabrication: making shapes without molds, Chemistry of Materials 9 (1997) 650–663.
[5] J.W. Halloran, M.Griffith, T.M.Chu, (Regents of the University of Michigan, Ann Arbor, Mich), 1997.
[6] T. Chartier, A. Badev, Y. Abouliatim, P. Lebaudy, L. Lecamp, Stereolithography process: Influence of the rheology of silica suspensions and of the medium on polymerization kinetics – Cured depth and width, Journal of the European Ceramic Society 32 (8) (2012) 1625–1634.
[7] X. Zhang, X. Jiang, C. Sun, Micro-stereolithography of polymeric and ceramic microstructures, Sensors and Actuators A 77 (2) (1999) 149–156.
[8] A. Bertsch, S. Jiguet, P. Renaud, Microfabrication of ceramic components by microstereolithography, Journal of Micromechanics and Microengineering 14 (2004) 197.
[9] V.K. Varadan, X. Jiang, V.V. Varadan, Microstereolithography and other fabrication techniques for 3D MEMS, John Wiley & Sons Inc, 2001.
[10] A. Bertsch, S. Jiguet, P. Bernhard, P. Renaud, Microstereolithography: a Review, in: materials Research Society symposia, Materials Research Society 758 (2003) 2–15.

[11] A. Goswami, A. Phani, A.M. Umarji, G. Madras, Polymer microfabrication by scanning based microstereolithography: optical design and material functionality, Review of Scientific Instruments 83 (9) (2012) 095003–095012.
[12] T. Chartier, C. Hinczewski, S. Corbel, UV curable systems for tape casting, Journal of the European Ceramic Society 19 (1) (1999) 67–74.
[13] C. Hinczewski, S. Corbel, T. Chartier, Stereolithography for the fabrication of ceramic three dimensional parts, Rapid Prototyping Journal 4 (3) (1998) 104–111.
[14] C. Provin, S. Monneret, Complex ceramic-polymer composite microparts made by microstereolithography, IEEE Transactions on Electronics Packaging Manufacturing 25 (1) (2002) 59–63.
[15] J.A. Lewis, Colloidal processing of ceramics, Journal of the American Ceramic Society 83 (10) (2000) 2341–2359.
[16] R.H. French, Origins and applications of London dispersion forces and hamaker constants in ceramics, Journal of the American Ceramic Society 83 (9) (2000) 2117–2146.
[17] L. Bergstrom, Collodal Processing of ceramics, in: K. Holmsberg (Ed.), Handbook of Applied Surface and Colloid Chemistry, John Wiley & Son, Ltd, 2001.
[18] I.D. Morrison, S. Ross, Colloidal Dispersions: Suspensions, Emulsions, and Foams, Wiley, 2002.
[19] A. Goswami, G. Srivastava, A.M. Umarji, G. Madras, Thermal degradation kinetics of poly(trimethylol propane triacrylate)/poly(hexane diol diacrylate) interpenetrating polymer network, Thermochimica Acta 547 (0) (2012) 53–61.
[20] V. Tomeckova, J.W. Halloran, Flow behavior of polymerizable ceramic suspensions as function of ceramic volume fraction and temperature, Journal of the European Ceramic Society 31 (14) (2011) 2535–2542.
[21] B.A. Horri, P. Ranganathan, C. Selomulya, H. Wang, A new empirical viscosity model for ceramic suspensions, Chemical Engineering Science 66 (12) (2011) 2798–2806.
[22] F. Gao, S. Yang, P. Hao, J.R.G. Evans, Suspension stability and fractal patterns: a comparison using hydroxyapatite, Journal of the American Ceramic Society 94 (3) (2011) 704–712.
[23] W.D. Teng, M.J. Edirisinghe, J.R.G. Evans, Optimization of dispersion and viscosity of a ceramic jet printing ink, Journal of the American Ceramic Society 80 (2) (1997) 486–494.
[24] D.-M. Liu, Particle packing and rheological property of highly-concentrated ceramic suspensions:φm determination and viscosity prediction, Journal of Materials Science 35 (2000) 5503–5507.
[25] T.Y. Kong, A.W. Roscoe, A Rosenfeld, Concepts of digital topology, Topology and its Applications 94 (3) (1992) 219.
[26] N. Sladoje, I. Nyström, P. Saha, Perimeter and Area Estimations of Digitized Objects with Fuzzy Borders, in: I. Nyström, G. Sanniti di Baja, S. Svensson (Eds.), Discrete Geometry for Computer Imagery, vol. 2886, Springer, Berlin Heidelberg, 2003, pp. 368–377.
[27] S. Dhara, P. Bhargava, Influence of nature and amount of dispersant on rheology of aged aqueous alumina gelcasting slurries, Journal of the American Ceramic Society 88 (3) (2005) 547–552.
[28] D. Gardini, M. Deluca, M. Nagliati, C. Galassi, Flow properties of PLZTN aqueous suspensions for tape casting, Ceramics International 36 (5) (2010) 1687–1696.
[29] Y.S. Lee, N.J. Wagner, Dynamic properties of shear thickening colloidal suspensions, Rheology Acta 42 (2003) 199–208.
[30] D.R. Foss, J.F. Brady, Structure, diffusion and rheology of Brownian suspensions by Stokesian dynamics simulation, Journal of Fluid Mechanics 407 (2000) 167–200.
[31] T.M.G. Chu, J.W. Halloran, High-temperature flow behavior of ceramic suspensions, Journal of the American Ceramic Society 83 (9) (2000) 2189–2195.